

# Quasi-periodic oscillations in superfluid magnetars

A. Passamonti<sup>1\*</sup>, S. K. Lander<sup>2†</sup>

<sup>1</sup> *INAF - Osservatorio Astronomico di Roma, Via Frascati 33, 00044 Rome, Italy*

<sup>2</sup> *Theoretical Astrophysics, University of Tübingen, Auf der Morgenstelle 10, D-72076 Tübingen, Germany*

8 November 2021

## ABSTRACT

We study the time-evolution of axisymmetric oscillations of superfluid magnetars with a poloidal magnetic field and an elastic crust, working in Newtonian gravity. Extending earlier models, we study the effects of composition gradients and entrainment on the magneto-elastic wave spectrum and on the potential identification of the observed quasi periodic oscillations (QPOs). We use two-fluid polytropic equations of state to construct our stellar models, which mimic realistic composition gradient configurations. The basic features of the axial axisymmetric spectrum of normal fluid stars are reproduced by our results and in addition we find several magneto-elastic waves with a mixed character. In the core, these oscillations mimic the shear mode pattern of the crust as a result of the strong dynamical coupling between these two regions. Incorporating the most recent entrainment configurations in our models, we find that they have a double effect on the spectrum: the magnetic oscillations of the core have a frequency enhancement, while the mixed magneto-elastic waves originating in the crust are moved towards the frequencies of the single-fluid case. The distribution of lower-frequency magneto-elastic oscillations for our models is qualitatively similar to the observed magnetar QPOs with  $\nu < 155\text{Hz}$ . *In particular, some of these QPOs could represent mixed magneto-elastic oscillations with frequencies not greatly different from the crustal modes of an unmagnetised star.* We find that many QPOs could even be accounted for using a model with a relatively weak polar field of  $B_p \simeq 3 \cdot 10^{14}\text{G}$ , because of the superfluid enhancement of magnetic oscillations. Finally, we discuss the possible identification of 625 and 1837 Hz QPOs either with non-axisymmetric modes or with high-frequency axisymmetric QPOs excited by crustal mode overtones.

**Key words:** MHD-stars: magnetic fields – stars: neutron – stars: oscillations

## 1 INTRODUCTION

Magnetars are a class of highly magnetised, slowly rotating neutron star. In contrast to typical rotation-powered pulsars, a magnetar’s magnetic field is believed to provide the energy reservoir needed to explain its quiescent activity and flaring episodes (Thompson & Duncan 1996). Most spectacularly, three of these stars have been seen to suffer giant flares, with energy output up to around  $10^{47}$  erg. In the aftermath of the more recent two observations, the data have been good enough to reveal the presence of quasi-periodic oscillations (QPOs) in the X-ray tail following the initial outburst. These QPOs span a rather wide range of frequencies, from tens of Hz up to kHz, and many are only detected

in short parts of the tail, which itself lasts for hundreds of seconds (Israel et al. 2005; Strohmayer & Watts 2005).

These observations appear to represent the first direct detection of neutron star oscillations and hence should contain information about the star’s equation of state (EoS), internal magnetic field configuration and so on. The problem is disentangling the contributions of these different aspects of the star’s physics given the limited available data; a flurry of papers since the original detections have aimed to do just that, through theoretical modelling of magnetar oscillations. Initially several studies focused on either the purely crustal oscillation problem (see e.g. Duncan 1998; Samuelsson & Andersson 2007) or the magnetic mode interpretation by using different models and techniques (see e.g. Levin 2007; Sotani et al. 2008; Cerdá-Durán et al. 2009; Colaiuda et al. 2009). A relevant result found by Levin (2007) and confirmed by other studies was that the spectrum of torsional Alfvén oscillations in a star with a purely poloidal field is

\* E-mail: andrea.passamonti@oa-roma.inaf.it

† E-mail: samuel.lander@uni-tuebingen.de

not discrete but consists of bands of continua. Magnetised models with a crust show a strong interaction between the magnetic and elastic waves (Glampedakis et al. 2006; Levin 2006), which form a single family of hybrid magneto-elastic oscillations (for a more detailed description of the literature see Sec. 5).

With general agreement about the oscillations of a single-fluid magnetar, attention has returned to the effect of neutron superfluidity on Alfvén oscillations. Earlier qualitative studies predicted that superfluidity would serve to increase the frequencies of magnetar QPOs with respect to those of a single-fluid model (van Hoven & Levin 2008; Andersson et al. 2009). We confirmed this through numerical simulations, focusing on non-axisymmetric modes in a magnetar core (Passamonti & Lander 2013). Our results suggested that the higher-frequency observed QPOs could be interpreted as Alfvén core modes, and we conjectured that matching our core model to an elastic crust could allow for a set of low-frequency magneto-elastic modes too, thus accounting for the wide range of frequencies observed. This was very recently confirmed by Gabler et al. (2013), in the simplest case where the neutron fluid is totally decoupled from the charged (proton plus electron) fluid in the core. This study found constant-phase oscillations, indicating that the QPO spectrum of a superfluid star can become effectively discrete at typical magnetar field strengths  $B_p \sim 10^{15}$  G, where  $B_p$  is the magnetic field at the pole.

The neutron superfluid in a neutron star is likely to be coupled to the proton fluid to some degree, through entrainment (Sauls 1989). For strong entrainment, in fact, the dynamics of the system would return to that of a single-fluid model. Another important aspect of multifluid physics in a neutron star is the non-constant ratio of protons to neutrons; protons make up a smaller fraction of the outermost part of the core than they do deeper in the star. It is therefore important to check what influence these effects have on the star’s oscillation spectrum.

Our aim in this paper is to include these two pieces of physics and hence make a fuller study of superfluid effects on magnetar QPOs. This work focuses on axisymmetric oscillations and is intended to be complementary to our earlier work on non-axisymmetric magnetar QPOs (Passamonti & Lander 2013). We begin by discussing our unperturbed background models, followed by the perturbation equations for a magnetised multifluid star with an elastic crust and the time-evolution code we use to solve them. Next, we confirm that our code reproduces earlier results for magnetar QPOs in the single-fluid limit, before moving on to studying two representative models for superfluid magnetars. Finally, we compare our results to the observations and discuss key outstanding issues in magnetar QPO modelling.

## 2 EQUATIONS OF MOTION

Three particle species are essential ingredients in a model neutron star: neutrons, protons and electrons. These appear in different guises in different regions of the star, depending on the local density and temperature. In the crust, protons and a fraction of neutrons are bound in a lattice of nuclei which become progressively heavier towards the bottom of the crust. When the density exceeds approximately  $4.3 \times$

$10^{11}$  g cm<sup>-3</sup>, neutrons may drip out of the nuclei and, if the temperature is below about  $10^9$  K, form a gas of superfluid neutrons. Also below this temperature, the neutrons and protons of the core are expected to become, respectively, superfluid and superconducting.

The dynamics of a superfluid neutron star are therefore more complex than a single-fluid model. However, the number of degrees of freedom can be reduced, if we note that the electromagnetic force locks together the various charged particles on very short timescales compared with the typical mode oscillation periods. This means that the charged particles can then be considered as a single neutral conglomerate of comoving particles.

A basic superfluid neutron star can therefore be studied from a dynamical point of view as a two-fluid system. In the core, the two constituents are the superfluid neutrons and a neutral mixture of charged particles that for simplicity we call ‘protons’. These two-fluid constituents are, respectively, denoted with n and p. Although the core protons are likely to be superconducting, we regard them as a normal fluid in this work, where our focus is rather the effect of neutron superfluidity on magnetar QPOs. In the inner crust, we may discern a fraction of free superfluid neutrons which permeates the lattice of nuclei, in which protons and the remaining part of neutrons are confined. These two crust constituents are denoted with f and c for, respectively, free superfluid neutrons and confined baryons.

Assuming we have small perturbations away from equilibrium, we may make the usual separation of the full system of equations for two-fluid magnetohydrodynamics (MHD) into a set governing the stationary background star and a set of time-evolution equations for the perturbations. We will see that, within our approximations, the background models are purely fluid with the two species fully decoupled; entrainment and elastic terms enter only at the order of the perturbations. We discuss solving the background and perturbation equations in turn in the next sections.

## 3 BACKGROUND MODELS

The background models are constructed as described in Lander et al. (2012). These are self-consistent multipolar solutions, accounting for the back-reaction of the magnetic field on the stellar fluid. The basic effect of neutron superfluidity, decoupling the protons and increasing the Alfvén mode frequencies, may be accounted for with a basic single-fluid unstratified background. However, we wish to explore the effect of more realistic configurations: stratification (i.e. a non-constant proton fraction), entrainment and a two-fluid core matched to a single-fluid crust.

We consider stellar models based on a two-fluid polytropic EoS, with an energy functional  $\mathcal{E}$  given by

$$\mathcal{E} = k_n \rho_n^{1+1/N_n} + k_p \rho_p^{1+1/N_p}, \quad (1)$$

where  $k_x$  are constants and  $N_x$  are the polytropic indices for each species. This simple EoS allows us to construct models with composition stratification by choosing different polytropic indices for protons and neutrons,  $N_p \neq N_n$ . Our models consist of a fluid core and an elastic crust, with the crust-core boundary at  $r_{cc} = 0.9R$ , where  $R$  is the star’s radius. Since we assume that the crust is relaxed for the

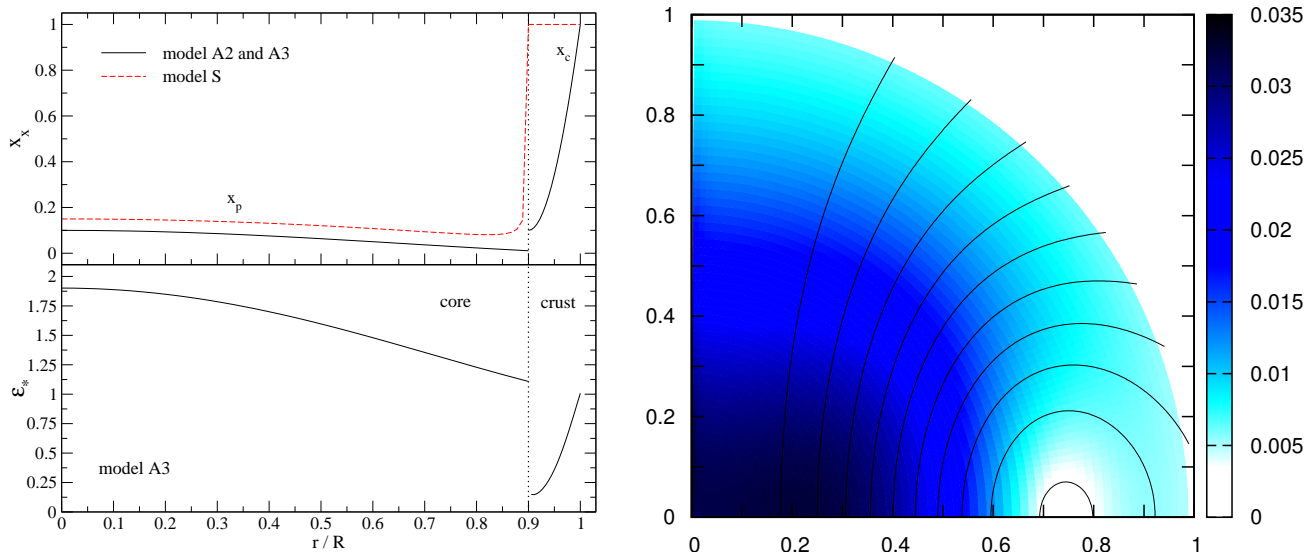


**Figure 1.** The upper-left panel shows the proton fraction profile used for models A2 and A3 (solid black line), and for model S (dashed red line). The lower-left panel displays the entrainment parameter  $\epsilon_*$  for model A3. Note that  $\epsilon_* = 1$  represents a two-fluid limit with completely decoupled neutral and charged particles, whilst  $\epsilon_* = x_c$  represents total coupling between them. The right-hand panel shows the magnetic field magnitude and direction of model S, with a two-fluid core and single-fluid crust. The crust/core transition is at  $r_{cc} = 0.9R$ . The magnetic field configuration for the unstratified model A1 is similar, with the closed field line region slightly further out.

background configurations the equations reduce to those of a purely fluid model; elastic terms enter only into the perturbation equations.

In this paper we aim to study oscillations of two ‘representative’ model magnetars, encapsulating the real physics of the system as best our framework allows. In addition, we will also need to investigate intermediate cases, in order to track modes from the well-studied single-fluid regime into new superfluid territory.

For basic tests, we use an unstratified model in which  $N_p = N_n = 1$ , and the proton and confined baryon fraction is  $x_p = x_c = 0.1$ . This model has been already used in literature (see for instance Passamonti et al. 2009), and we term it ‘model A1’.

We generalise this model A1 by adding an ‘artificial’ composition gradient both in the core and the crust. The relations for  $x_p$  and  $x_n$  try to mimic the profile expected in more realistic models, where the proton fraction decreases from the centre to the crust/core transition and the confined baryon fraction increases into the inner crust up to unity at the neutron drip transition. This is not fully consistent, but for a pure-poloidal magnetic field geometry the axial modes are decoupled from the polar sector and the only background quantity that appears in the dynamical equations is the mass density. Therefore, this is a ‘controlled’ inconsistency that is quite appropriate for the aims of our current work. More specifically, we consider  $x_p = 0.1\rho$  in the core and  $x_c = 1 + a\rho + b\rho^2$  in the crust, where  $a$  and  $b$  are two constants that depend on the value of  $x_c$  and its derivative at  $r_{cc}$ . We call this particular configuration ‘model A2’ and its composition stratification is shown in Fig. 1.

Another property that characterises superfluid neutron stars is the entrainment, which is a non-dissipative process that couples the dynamics of protons and superfluid neu-

trons. This effect is due to the strong interaction which limits the free motion of each individual particle species. The entrainment can be described, from the dynamical point of view, in terms of an effective nucleon mass which replaces its own ‘bare’ mass in the dynamical equations (Sauls 1989). Although our background models are non-rotating, this quantity affects the dynamics of linear perturbations; see Sec. 4. At the bottom of the inner crust, the effective mass of superfluid neutrons may be quite large  $m_n^* \simeq 14m_n$ , where  $m_n$  is the neutron bare mass. This strong entrainment originates from the neutron Bragg scattering from the nuclei lattice (Chamel 2012). In a core with superfluid/superconducting constituents, the neutron effective mass typically is  $0.92 \lesssim m_n^*/m_n \lesssim 1$  (Chamel 2008). Although we consider normal core protons in our stellar models, we investigate also configurations with non-zero core entrainment to estimate the effect on the spectrum; note that in this case one should include proton superconductivity, so our core magnetar model is not strictly consistent. We introduce the effects of entrainment in our model by using the approximation to the effective mass profile determined by Chamel (Passamonti & Andersson 2012). We form one of our two key test models, denoted ‘model A3’, by using this entrainment profile with the same composition gradient described above for model A2. The entrainment profile is shown in figure 1.

We also study a model with two fluids in the core and only a single fluid in the crust. This model, which we call ‘model S’, is obtained by choosing  $N_p = 1.3$  and  $N_n = 0.6$ . In this case we set the central proton fraction  $x_p(r=0) = 0.15$ . The resultant  $x_p$  profile partially mimics the imposed profile from the previous model, but within a fully self-consistent framework; this is shown, together with the magnetic field configuration, in figure 1. This model S can be thought of as

a young magnetar which has a superfluid core and a normal crust, i.e. a star in which the crust's temperature is still above the neutron critical temperature (Ho et al. 2012). This model can be also considered an approximation to a star with a strong entrainment in the inner crust, in which the motion of the free superfluid neutrons is almost comoving with the confined baryons of the crustal lattice.

We provide our results in dimensionless units which are constructed from the gravitational constant,  $G$ , the total central mass density,  $\rho_0$ , and the star's radius,  $R$ . The dimensionless masses for models A and S are, respectively,  $M = 1.273\rho_0 R^3$  and  $M = 1.391\rho_0 R^3$ . The crust/core transition is at  $r_{cc} = 0.9R$  where the dimensionless mass density is  $\rho_{cc} = 0.109\rho_0$  and  $0.009\rho_0$  for models A and S, respectively. The differences in the values of  $\rho_{cc}$  reflect the fact that our toy double-polytrope models cannot reproduce all features of a tabulated EoS.

#### 4 PERTURBATIONS

Let us now derive the evolution equations of axisymmetric ( $m = 0$ ) perturbations, where  $m$  is the azimuthal number. For a purely poloidal or toroidal magnetic field, axisymmetric oscillations can be decoupled in polar and axial perturbations. The polar sector describes compressible oscillations which are driven by the radial and theta velocity components and the density perturbation. The axial perturbations instead describe an incompressible motion along the azimuthal coordinate, which can be completely characterised for each species by the single velocity component  $\delta v_x^\phi$ , where the index 'x' denotes the fluid constituents: p and n in the core, c and f in the crust.

In this work, we focus on the axial sector, which is considered the most relevant for magnetar QPOs: the oscillation frequencies appear better matched to the observations (at least in the single-fluid case) and, being incompressible, the axial modes can be excited with a smaller energy (Duncan 1998). However, polar perturbations should not be completely neglected in a more general magnetar model. In fact, in stars with a general mixed poloidal-toroidal magnetic field, the axial and polar sectors couple and the mode spectrum can be considerably affected (Colaiuda & Kokkotas 2012). In addition, polar perturbations might be relevant for understanding the QPOs observed at higher frequencies. We intend to study these modes in a future paper.

In a superfluid and magnetised neutron star, the dynamics of axial oscillations can be described by momentum conservation equations for each fluid constituent and by the induction equation (Glampedakis, Andersson & Samuelsson 2011). The mass conservation and Poisson equations are automatically satisfied due to the incompressibility of the axial perturbations,  $\Delta\rho = \delta\rho = 0$ , where  $\Delta$  and  $\delta$  denote, respectively, the Lagrangian and Eulerian perturbations. Since the axial oscillations of a non-rotating superfluid star with a purely poloidal magnetic field are characterised by the  $\phi$  component of the velocity and magnetic field perturbations, we omit the coordinate index from all perturbation variables. Therefore  $\delta v$  and  $\delta B$  stand for  $\delta v^\phi$  and  $\delta B^\phi$ , respectively.

The superfluid neutrons of the core in a non-rotating

star obey the following equation:

$$(1 - \varepsilon_n) \frac{\partial \delta v_n}{\partial t} + \varepsilon_n \frac{\partial \delta v_p}{\partial t} = 0, \quad (2)$$

where the parameter  $\varepsilon_x$  accounts for the entrainment between the nucleons. As already pointed out in Sec. 3 the entrainment describes the relative dragging that a fluid constituent induces on the other component. This entrainment parameter is related to the effective mass by  $\varepsilon_x = 1 - m_x^*/m_x$ .

To study the dynamics of an elastic crust it is more suitable to introduce the Lagrangian displacement for each fluid constituent (Andersson et al. 2011), which is defined in a non-rotating star by the following expression:

$$\frac{\partial \xi_x^i}{\partial t} = \delta v_x^i. \quad (3)$$

Equation (2) therefore can be re-written as follows

$$\frac{\partial^2 \xi_n}{\partial t^2} = \frac{\varepsilon_n}{\varepsilon_n - 1} \frac{\partial^2 \xi_p}{\partial t^2}. \quad (4)$$

The free neutron gas of the inner crust obeys the same equation (4) provided we replace the symbols n with f and p with c.

In the ideal MHD approximation and for non-superconducting protons, the oscillations of the p-fluid in the core are restored by the Lorentz force, and the momentum equation reads

$$(1 - \varepsilon_p) \frac{\partial^2 \xi_p}{\partial t^2} + \varepsilon_p \frac{\partial^2 \xi_n}{\partial t^2} = \delta \left( \frac{f_L}{\rho_p} \right)^\phi. \quad (5)$$

The confined baryons of the crust interact with the magnetic field via the Lorentz force but can also sustain shear waves due to the elasticity of the ion lattice. Consequently, the dynamical equation for the confined constituent is given by

$$(1 - \varepsilon_c) \frac{\partial^2 \xi_c}{\partial t^2} + \varepsilon_c \frac{\partial^2 \xi_f}{\partial t^2} = \delta \left( \frac{f_L}{\rho_c} \right)^\phi + \frac{1}{\rho_c} \nabla^j \sigma_j^\phi, \quad (6)$$

where the elastic stress tensor is defined by

$$\sigma_{ij} = \mu (\nabla_i \xi_j^c + \nabla_j \xi_i^c) - \frac{2}{3} \mu (\nabla^k \xi_k^c) \delta_{ij}, \quad (7)$$

and  $\mu$  is the elastic shear modulus. For the crust's shear modulus, we use the approximate relation

$$\mu = \alpha \rho, \quad (8)$$

which is based on the observation that the specific shear modulus is almost constant through the crust with  $\alpha \simeq 10^{16} \text{ cm s}^{-1}$  (Douchin & Haensel 2001).

Next, by using Ampère's law to replace the electric current, the Lorentz force assumes the following form:

$$f_i^L = \frac{B^j}{4\pi} (\nabla_j B_i - \nabla_i B_j), \quad (9)$$

while the evolution of the magnetic field is described by the induction equation:

$$\partial_t \delta B_i = \epsilon^{ijk} \epsilon_{klm} \nabla_j (\delta v_p^l B^m). \quad (10)$$

In the crust, the proton velocity must be replaced with  $\delta v_c$ , i.e. the velocity perturbation of the confined fluid component.

The dynamical problem of the axial axisymmetric oscillations of a superfluid magnetised star with crust can be

studied with a single wave equation for the proton component in the core and the confined baryons in the crust, as in the single-fluid model. Focusing for a moment on the crust, the first step to derive this wave equation is to use equation (4) for the crust constituents and remove in equation (6) the superfluid neutron variable  $\xi_f$ . Equation (6) can then be written as follows:

$$\varepsilon_\star^{-1} \frac{\partial^2 \xi_c}{\partial t^2} = \delta \left( \frac{f_L}{\rho_c} \right)^\phi + \frac{1}{\rho_c} \nabla^j \sigma_j^\phi, \quad (11)$$

where  $\varepsilon_\star$  is a new parameter that accounts for entrainment defined by

$$\varepsilon_\star \equiv \frac{1 - \varepsilon_f}{1 - \varepsilon_f - \varepsilon_c}. \quad (12)$$

This new entrainment parameter can be written in terms of the effective mass (Andersson et al. 2009):

$$\varepsilon_\star = x_c \left( 1 - x_f \frac{m_f}{m_f^\star} \right)^{-1}. \quad (13)$$

The zero entrainment case in which protons and neutrons are entirely decoupled is given by  $\varepsilon_\star = 1$ . The entirely coupled ‘one-fluid’ limit where protons and neutrons comove is given by the  $m_f/m_f^\star \rightarrow 0$  limit which leads to  $\varepsilon_\star = x_c$ .

The second step is to perturb the Lorentz force (9) and use the time integration of equation (10) to replace the perturbation of the magnetic field  $\delta B$  with the Lagrangian displacement  $\xi_c$ . After some calculation, one may show that the c component obeys the following wave equation:

$$\begin{aligned} \rho_c \varepsilon_\star^{-1} \frac{\partial^2 \xi_c}{\partial t^2} = & A_1 \frac{\partial^2 \xi_c}{\partial r^2} + A_2 \frac{\partial^2 \xi_c}{\partial \theta^2} + A_3 \frac{\partial^2 \xi_c}{\partial r \partial \theta} \\ & + A_4 \frac{\partial \xi_c}{\partial r} + A_5 \frac{\partial \xi_c}{\partial \theta} + A_6 \xi_c \end{aligned} \quad (14)$$

where the  $A_k$  coefficients depends on the background variables and are given in the appendix. The core’s protons obey the same wave equation with the coefficients  $A_k$  taken in the zero shear modulus limit,  $\mu = 0$ .

#### 4.1 Boundary conditions

The regularity condition for equation (14) and the variable  $\xi_p$  at the centre ( $r = 0$ ) lead to a zero condition for the Lagrangian displacement  $\xi_p = 0$ . For axial axisymmetric perturbations the variable  $\xi_p$  and  $\xi_c$  also vanish at the magnetic symmetry axis.

At the core/crust interface, we need to impose the continuity of the  $\phi$  component of the Lagrangian displacement (Andersson et al. 2011)

$$\xi_p = \xi_c \quad (15)$$

and the continuity of the traction. For a purely poloidal magnetic field and non-rotating star, the  $\phi$  component of the traction in the crust is given by

$$\delta t^\phi = (\mu + B_r^2) \left( \frac{\partial \xi_c}{\partial r} - \frac{\xi_c}{r} \right) + \frac{B^r B^\theta}{r} \left( \frac{\partial \xi_c}{\partial \theta} - \cot \theta \xi_c \right), \quad (16)$$

while in the core it assumes the same form provided we replace the index c with p and set a zero shear modulus ( $\mu = 0$ ). From equation (15) and the continuity of the magnetic field across the interface, the traction condition reads

$$B_r^2 \frac{\partial \xi_p}{\partial r} = (\mu + B_r^2) \frac{\partial \xi_c}{\partial r} - \mu \frac{\xi_c}{r}. \quad (17)$$

At the surface of the star our evolutions must satisfy a zero traction condition ( $\delta t^\phi = 0$ ).

With respect to the equatorial plane, the axial ( $m = 0$ ) perturbations divide in a symmetric and anti-symmetric class. The symmetric oscillation modes satisfy  $\partial_\theta \xi_x = 0$  at  $\theta = \pi/2$ , while the anti-symmetric modes obey  $\xi_x = 0$ .

#### 4.2 Numerical method

The wave equation (14) is evolved in time on a two-dimensional grid which covers the first quadrant of the  $(r, \theta)$  plane, i.e.  $0 \leq r \leq R$  and  $0 \leq \theta \leq \pi/2$ . This restriction to the first quadrant is feasible due to the equatorial reflection symmetries of the axial  $m = 0$  oscillations.

The spatial derivatives are discretised by using a second order approximation, while the time integration of equation (14) is carried out by using an explicit iterative Crank-Nicholson method. We use various grid resolutions to test our results and have also used meshes with finer resolution in the crust in order to describe properly the shear waves. However, the results shown in this paper have been determined with an evenly spaced grid with resolution  $48 \times 90$ , respectively, in the  $\theta$  and  $r$  coordinates. To stabilise the simulations from high-frequency noise, we add an artificial fourth-order Oliger-Kreiss dissipation term,  $\varepsilon_D D_4 \xi$ , with a small dissipation coefficient  $\varepsilon_D \sim 10^{-5}$ .

The junction conditions (15) and (17) at the crust/core interface are used to determine at any time step the value of  $\xi_x$  at  $r_{cc}$ . This is obtained by discretising equation (17) with a side-stencil derivative both in the core and the crust region and then using equation (15).

#### 4.3 Initial conditions

The initial data of our time evolutions are a linear combination of various shear mode eigenfunctions of an unmagnetised star which are determined with an eigenfrequency code (Passamonti & Andersson 2012). These eigenfunctions are prolonged into the core by matching them continuously with polynomial functions in the radial coordinate. The angular part of the initial data must obey the boundary conditions described in Sec. 4.1.

### 5 QPO SPECTRUM

In magnetars, the QPO spectrum is believed to originate from magneto-elastic waves which arise from the dynamical interaction between the global magnetic field oscillations and the shear waves of the crust. The strong magnetic field of magnetars in fact efficiently couples the dynamics of the core and the crust, and the families of the shear and Alfvén modes are not independent anymore. It is more appropriate to consider them as a unique class of magneto-elastic oscillations.

Many of the observed QPO frequencies fall in the range  $\nu < 100\text{Hz}$ , suggesting that they may be generated by oscillations with axial parity and symmetry. This hypothesis is also supported by the minor energy required to excite the axial and axisymmetric modes, making them more suitable for the QPO seismic origin interpretation.

**Table 1.** This table displays the frequencies of the first three axial shear modes determined with the current time domain evolution (TD) and with the frequency domain (FD) approach. The mode frequencies for the  $l = 2, 3, 4$  multipoles are shown in dimensionless units  $\nu/\sqrt{G\rho_0}$  for an unstratified model with constant component fraction  $x_p = x_c = 0.1$  and with no magnetic field. The results obtained with these two different approaches agree to within a few percent.

$l$	${}^l t_0$	TD		FD		
		${}^l t_1$	${}^l t_2$	${}^l t_0$	${}^l t_1$	${}^l t_2$
2	0.0109	0.1920	0.3539	0.0108	0.1906	0.3514
3	0.0177	0.1982	0.3631	0.0170	0.1914	0.3517
4	0.0228	0.1986	0.3638	0.0229	0.1920	0.3520

As originally shown by Levin (2007), magnetic axial-axisymmetric oscillations form bands of continuous spectra which, depending on the magnetic field strength, efficiently absorb the shear modes of the crust whose frequencies lie inside the continuum. In an ideal system, the Alfvén continuum is generated by the independent motion of each magnetic field line with its own particular oscillation frequency. Several studies have shown that long-lived oscillations exist at both the turning points and the edges of the continuum (Cerdá-Durán et al. 2009; Colaiuda et al. 2009; van Hoven & Levin 2011). For instance, in neutron stars with a purely poloidal magnetic field, long-lived oscillations should appear both in the region of open and closed field lines. In the former sector, two families of QPOs have typically been identified for each continuum band, namely a lower  $L_n$  oscillation near the last open field line and an upper  $U_n$  wave near the pole. Each class can be further divided into symmetric and anti-symmetric oscillations with respect to the equatorial plane (see Sec. 4.1). Symmetric and anti-symmetric QPOs will be, respectively, denoted with the (+) and (−) upper indices.

Another distinct class of QPOs is instead associated with the motion of the closed magnetic field lines, which we call  $C_n$  following Colaiuda et al. (2009). Differently from the  $L_n$  and  $U_n$  families the  $C_n$  QPOs do not have a preferred symmetry at the equatorial plane, i.e. they appear in the spectrum in both cases with equal frequency. We omit therefore to specify the  $C_n$  oscillation symmetry in the rest of this work.

Note that the literature on this subject has not been consistent with notation conventions — for instance, in Gabler et al. (2012) the lower QPOs are called the edges of the continuum and denoted as  $E_n$ , while the  $C_n$  are represented with  $L_n$ .

The inclusion of an elastic crust allows for shear waves which interact with the magnetic field. Within the models described above — axial axisymmetric oscillations of single-fluid stars — shear modes with frequencies inside the continuous spectrum are absorbed efficiently by Landau damping within a second or less, while shear modes that lie outside may persist longer. In any case, the shear modes become magneto-elastic: their mode frequency and eigenfunction pattern are both modified by the field (Gabler et al. 2011; van Hoven & Levin 2012).

In a more general magnetic field geometry, like one with a mixed poloidal-toroidal field configuration, the toroidal field component may couple oscillations with polar and axial

**Table 2.** Frequencies for the first three  $l = 2$  axial shear modes for an unstratified model with  $x_p = 0.1$ , zero magnetic field and with a strong crust entrainment as determined by Chamel (2012). The first column shows the value of the confined baryon fraction in the crust, while TD and FD stand, respectively, for time and frequency domain approach. The time evolutions accurately reproduce the scaling of the mode frequencies with the entrainment.

$x_c$	${}^2 t_0$	TD		FD		
		${}^2 t_1$	${}^2 t_2$	${}^2 t_0$	${}^2 t_1$	${}^2 t_2$
0.1	0.00347	0.0669	0.1219	0.00368	0.0659	0.1200
0.5	0.00324	0.0638	0.1181	0.00356	0.0631	0.1158

parity, leading to a more complex spectrum. In particular, it is expected that the continuum bands will be destroyed by this coupling and the spectrum should appear discrete (Colaiuda & Kokkotas 2012).

### 5.1 Superfluid physics effects on the spectrum

Below the superfluid transition temperature  $T_c \simeq 10^9$  K, the dynamics of the superfluid neutrons and protons decouple. These two constituents in general do not comove and as a result the velocity of the Alfvén and shear waves now depend only on the proton/confined-baryon mass density:

$$v_A = \frac{B}{\sqrt{4\pi\rho_c}}, \quad v_s = \sqrt{\frac{\mu}{\rho_c}}. \quad (18)$$

Since in the core of a neutron star  $x_p \ll 1$  and in the crust  $0.1 < x_c \leq 1$ , the Alfvén and shear modes of a superfluid system have higher frequencies than a normal matter neutron star.

The entrainment affects the relative motion between the two fluids and modifies the oscillation frequencies compared with a completely decoupled two-fluid system. A plane-wave approximation study (Andersson et al. 2009) showed that the Alfvén and shear mode frequencies in a superfluid star may be described by the following expression:

$$\sigma = \sqrt{\frac{\varepsilon_\star}{x_c}} \sigma_0, \quad (19)$$

where  $\sigma_0$  is the frequency determined in a normal, single fluid star and  $\varepsilon_\star$  is the entrainment parameter introduced in Sec. 4. In the neutron star’s core equation (19) changes with the usual replacement of  $x_c$  with  $x_p$ . Of course, whilst equation (19) provides a qualitative prediction for the scaling of magnetic and shear modes, which agrees very well with our numerical results for simple stellar models with no composition gradients, one needs to solve the perturbation equations to get quantitative results.

In our previous paper (Passamonti & Lander 2013) we performed time evolutions of non-axisymmetric perturbations, for purely fluid magnetar models. For reasonable values of  $\varepsilon_\star$ , the central proton fraction  $x_p(0)$  and the polytropic indices  $N_n, N_p$  we found that magnetic modes in a superfluid magnetar were shifted up in frequency rather dramatically, by a factor of 6 with respect to a non-superfluid star.

In this work, we add a crust to our superfluid magnetar models, specialising to axisymmetric oscillations in this

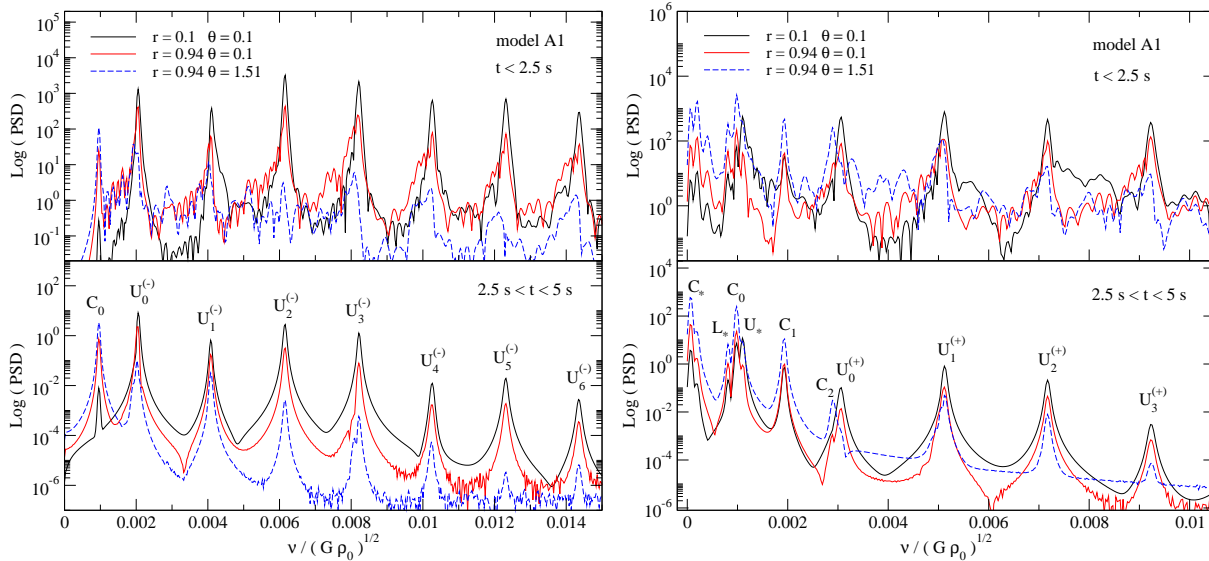


**Figure 2.** Spectrum of model A1 with  $x_p = x_c = 0.1$  and a poloidal dimensionless magnetic field  $B_p = 9.48 \cdot 10^{-4} \sqrt{G} \rho_0 R$ . For a typical neutron star with  $M = 1.4 M_\odot$  and  $R = 10 \text{ km}$  the magnetic field at the pole is  $B_p = 5.4 \cdot 10^{14} \text{ G}$ . This figure shows an FFT of the Lagrangian displacement  $\xi$  at three different points inside the star and for two periods of the time evolution. For the antisymmetric oscillations, the two left-hand panels display an FFT at  $(r, \theta) = (0.1, 0.1)$  (solid black line),  $(r, \theta) = (0.94, 0.1)$  (solid red line) and  $(r, \theta) = (0.94, 0.151)$  (dashed-blue line). The two right-hand panels show the same quantities for the symmetric waves. Furthermore, the FFTs performed for a period of  $t < 2.5 \text{ s}$  are shown in the two upper panels, while the two lower panels display the FFTs for the following time interval  $2.5 < t < 5 \text{ s}$ . The oscillation frequencies are given in dimensionless units.

**Table 3.** This table displays the frequencies of  $C_n$  and  $U_n$  oscillations for four stellar models with an averaged magnetic field  $\langle B \rangle = 10^{15} \text{ G}$ . This corresponds to a polar field  $B_p = 3.3 \cdot 10^{14} \text{ G}$  for model S and  $B_p = 5.4 \cdot 10^{14} \text{ G}$  for model A. The first column provides the stellar model, while the remaining columns show the oscillation frequencies in dimensionless units  $\nu / \sqrt{G \rho_0}$  and multiplied by  $10^3$ .

Model	$C_0$	$C_1$	$U_*$	$U_0^{(-)}$	$U_1^{(-)}$	$U_2^{(-)}$	$U_0^{(+)}$	$U_1^{(+)}$	$U_2^{(+)}$
S	1.33	2.61	0.61	1.11	2.21	3.40	1.62	2.82	3.98
A1	0.99	1.94	1.10	2.06	4.12	6.17	3.08	5.12	7.18
A2	1.86	3.70	1.24	2.58	5.29	7.69	3.91	6.48	9.37
A3	2.06	—	1.41	3.33	6.72	10.19	5.01	8.46	11.93

case. As well as allowing for modes restored by elastic forces, the entrainment profile of our stars will also be seriously affected. In contrast to the core, where entrainment is relatively weak, recent calculations show that the motion of superfluid neutrons in the inner crust may be strongly limited by Bragg scattering with the ion lattice. As a result, the neutron effective mass in the inner crust can be  $m_n^* \simeq 14 m_n$ . Due to this strong entrainment, the dynamics of the two fluids in the crust approaches that of a single-fluid system. As already calculated in non magnetised systems, the effect of a strong effective mass on the crustal modes is about a 10% correction of the non-superfluid case (Andersson et al. 2009; Samuelsson & Andersson 2009; Passamonti & Andersson 2012; Sotani et al. 2013). In the next section, we consider also models with this strong entrainment in the crust and study the effects on the magneto-elastic waves.

## 6 RESULTS

From the evolutions of equation (14), we determine the spectral properties of axial, axisymmetric oscillations in super-

fluid models of magnetars. We first test our numerical framework with simplified models and then study the oscillations of stars with composition gradients and entrainment.

### 6.1 Magneto-elastic waves in unstratified stars

We study in this section, the oscillation spectrum of a model A1 star, which is a two-fluid polytropic star with crust/core transition located at  $r_{cc} = 0.9R$ . The polytropic indices are  $N_x = 1$  both in the core and the crust, which means there is no composition gradient. Although it would be possible to choose a different constant composition fraction in the core and crust, we start for simplicity with a model where  $x_p = x_c = 0.1$ , which is qualitatively similar, from the point of view of the axial-axisymmetric spectrum, to the single fluid case ( $x_p = x_c = 1$ ). The only difference is that, as expected from equation (19), the oscillation frequencies are shifted to higher values due to the lower proton fraction.

To test our numerical simulations, we start with an unmagnetised model and determine the shear modes. We can compare the mode frequencies with the results obtained

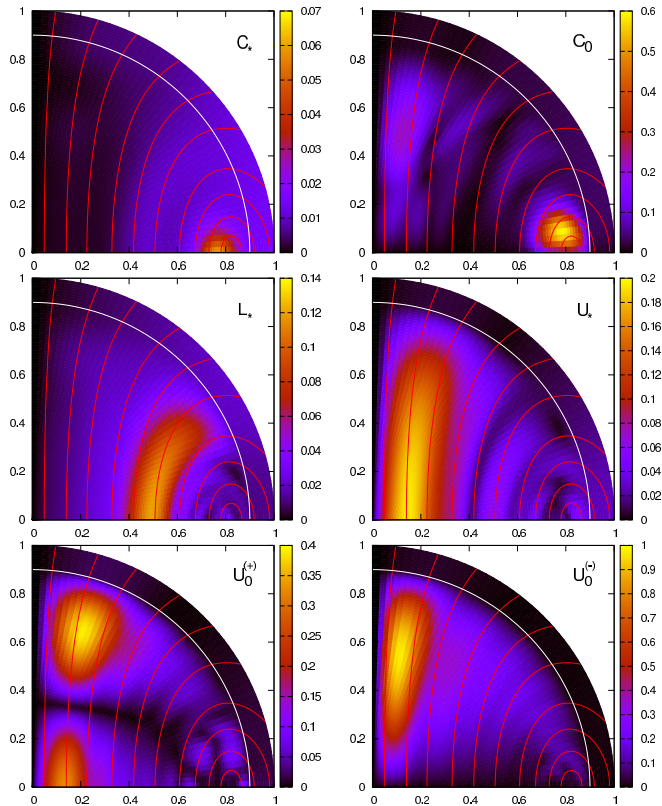


**Figure 3.** This figure shows the effective 2D-FFT of six magneto-elastic waves for a model A1 star with magnetic field  $B_p = 5.4 \cdot 10^{14}$  G. From the spectral features of Fig. 2 we select the following modes and show in the three left-hand panels (from the top):  $C_*$ ,  $L_*$  and  $U_0^{(+)}$ , and in the three right-hand panels (from the top):  $C_0$ ,  $U_*$  and  $U_0^{(-)}$ .

with a numerical code developed by Passamonti & Anderson (2012), which solves the spectrum of a superfluid neutron star with crust as an eigenvalue problem. The mode frequencies of the fundamental mode and the first two overtones are listed in Table 1 for the  $l = 2, 3$  and 4 multipoles. The results of the two approaches agree to better than a few percent. We assess the accuracy of our code also for different values of  $x_c$  and entrainment. For instance, we provide in Table 2, the frequency for two unstratified models, one with  $x_p = x_c = 0.1$  and the other with  $x_p = 0.1$  and  $x_c = 0.5$ , and both having a realistic entrainment profile (see Section 3).

As already pointed out in Sec. 3, we provide our results in dimensionless units. If not otherwise stated we translate any dimensionless quantity to physical values by using a fiducial stellar model with typical mass  $M = 1.4M_\odot$  and radius  $R = 10$  km.

The next step in our preliminary analysis is to add a poloidal magnetic field to the same model A1 with  $x_p = x_c = 0.1$ . We consider different magnetic field strength and study the spectrum with fast Fourier transformation (FFT) taken at different positions inside the numerical grid. This is a standard technique to recognise the continuum bands of the spectrum and the potential discrete modes. In Fig. 2, we show an example of an FFT of the Lagrangian displacement for a long evolution of about 5 s and for both symmetric and anti-symmetric equatorial conditions (see Sec. 4.1). This

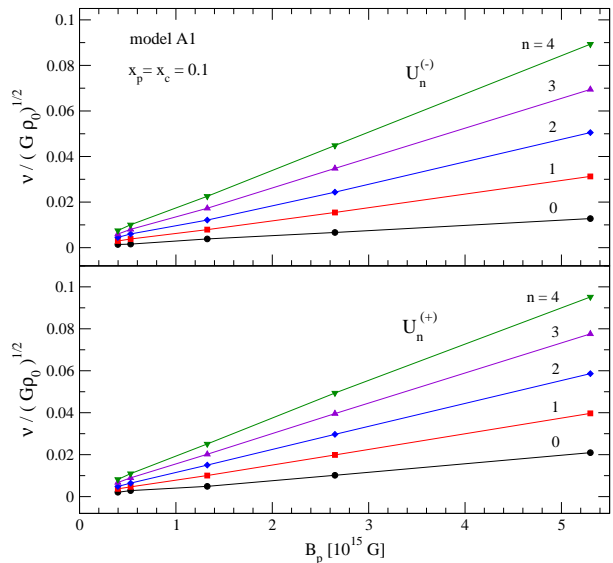


**Figure 4.** Variation of the  $U_n$  frequencies with polar magnetic field  $B_p$  for a model A1 with  $x_p = x_c = 0.1$ .  $B_p$  is shown on the horizontal axis in physical units for the fiducial model  $M = 1.4M_\odot$  and  $R = 10$  km. The upper and lower panels display, respectively, the antisymmetric and symmetric oscillations.

star has a magnetic field at the pole  $B_p = 9.48 \cdot 10^{-4} \sqrt{G \rho_0} R$  ( $B_p = 5.4 \cdot 10^{14}$  G for our fiducial model). To trace the energy transfer among the various modes, we perform an FFT in two distinct periods of the simulation before and after 2.5 s. It is clear from Fig. 2 that after an initial period where several oscillations are excited the system relaxes in a configuration in which only the  $U_n$  and  $C_n$  oscillations survive longer. This behaviour and the analysis of the FFT in other positions inside the star appear consistent with the presence of bands of continuous spectrum, in which long-lived oscillations can arise at the continuum edges, while oscillations inside the continuum are quickly damped.

To support the identification of the various magneto-elastic waves, we determine also an effective FFT in the whole 2D-numerical grid with a code developed by Stergioulas et al. (2004). Several  $C_n$  and  $U_n$  QPOs are easily identified and in addition we also find the symmetric QPO denoted as  $U_*$  by Gabler et al. (2012). At low frequencies, we find two symmetric magneto-elastic oscillations, which as far as we know, have not been reported before in the literature. We call them  $C_*$  and  $L_*$  and they are, respectively, associated with the closed and open field line regions. These magneto-elastic waves as well as  $U_*$  exist due to coupling with the crust. In a model without crust these oscillations would not conserve angular momentum (Cerdá-Durán et al. 2009). The effective 2D-FFT of these QPOs as well as of the first  $C_n$  and  $U_n$  oscillations are shown in Fig. 3.

We determine the variation of symmetric and anti-symmetric  $U_n$  QPOs with the magnetic field and show our results in Fig. 4. This figure also illustrates that we are able to recover the expected scaling in a neutron star with crust, i.e.  $U_n \simeq (1+n)U_0$  (Colaiuda & Kokkotas 2011).

Another method to determine the continuum/discrete nature of the spectrum is the study of the mode phase. In their superfluid models, Gabler et al. (2013) find QPOs with



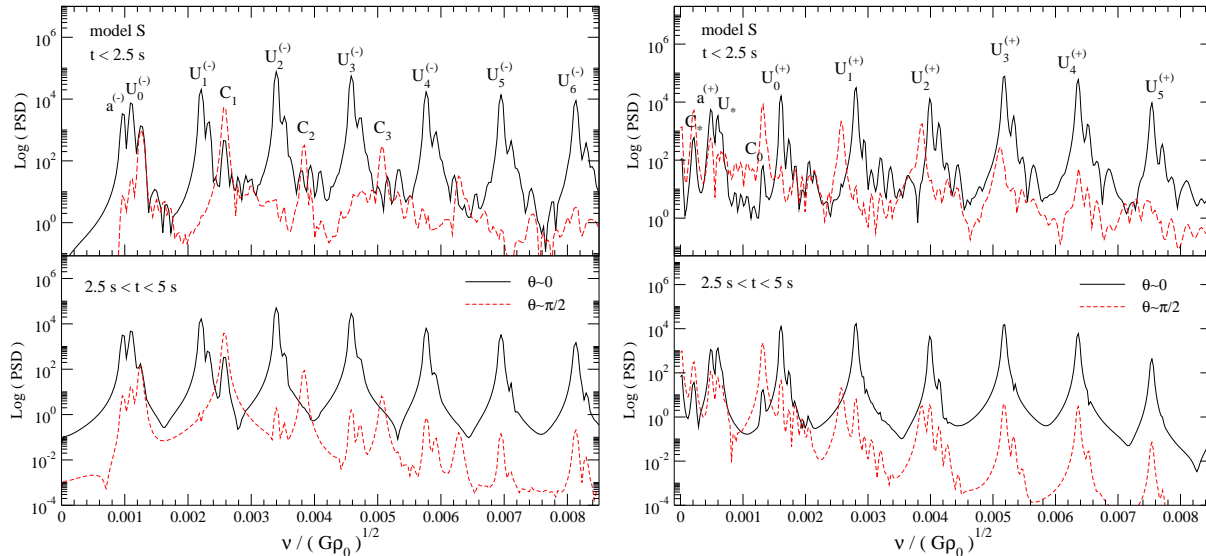


**Figure 5.** Axial axisymmetric spectrum of magneto-elastic waves for model S, which has composition gradients in the core. The magnetic field at the pole is  $B_p = 6.4 \cdot 10^{-4} \sqrt{G\rho_0} R$ . For a typical neutron star with  $M = 1.4M_\odot$  and  $R = 10\text{km}$  the magnetic field is  $B_p = 3.3 \cdot 10^{14}\text{G}$ . This figure displays the power spectrum of the Lagrangian displacement  $\xi$  taken inside the crust near the magnetic axis (solid-black lines) and equator (dashed-red lines). The two upper panels show FFTs taken within 2.5 s, while the two lower panels show FFTs taken during  $2.5 < t < 5$  s. Furthermore, the antisymmetric oscillations are shown in the left-hand panels and the symmetric ones in the right-hand panels.

constant phase when  $B_p \sim 10^{15}\text{G}$ , indicating that these are discrete modes. To investigate this issue, we studied an unstratified model A with  $x_p = 0.05$  and  $x_c = 1$  (single-fluid crust), i.e. with a composition fraction similar to that used by Gabler et al. (2013), and increased the numerical resolution to  $96 \times 120$  for, respectively, the  $\theta$  and  $r$  coordinates. Our results of the QPO phase, however, do not show convincing evidence of the continuum/discrete transition. This may be due to differences in the models and framework, but it is difficult to make detailed comparisons at this stage, given the brevity of the Gabler et al. (2013) paper. For the other superfluid models of this work (model S and A3), we studied the phase and found the same conclusions as for the unstratified model A.

In models in which either the component fraction or entrainment assumes the same constant value in the entire stellar volume, the spectrum is expected to shift globally at different frequencies. This is due to the same dependence of the Alfvén and shear modes on the proton fraction and entrainment (see equations 18 and 19). We have also tested the good behaviour of our numerical results by varying  $x_p = x_c$  and  $\epsilon_*$ , and found the expected mode frequency scaling. We do not report this test here as the scaling is very similar to the non-axisymmetric modes, which we have already considered in Passamonti & Lander (2013). Having confirmed that our code reproduces earlier results for magneto-elastic waves, we now move on to consider more realistic configurations.

## 6.2 Effects of composition stratification

The core and the crust of a neutron star have composition gradients which depend on the EoS. In general, in the core the proton fraction decreases from the star’s centre towards

the crust, while the fraction of confined baryons increases from the bottom of the crust up to the neutron drip density, where all the nucleons are locked in the nuclei and  $x_c = 1$ .

We first study the effects of composition stratification using our model S. As described in Sec. 3, this is a two-fluid system in the core which matches a single fluid in the crust (see Fig. 1), as a result it has composition gradients only in the core. This stratification has been determined by choosing two different polytropic indices for protons and neutrons, respectively,  $N_p = 1.3$  and  $N_n = 0.6$ . Considering the initial data introduced in Sec. 4.3, we provide a linear combination of the first  $l = 10$  multipoles of the fundamental axial shear modes  ${}^l t_0$  of a superfluid unmagnetised star. These modes reside in the lower frequency band of the spectrum and may potentially interact with the global magnetic waves. For a star with  $B_p = 3.3 \cdot 10^{14}\text{G}$  and average magnetic field  $\langle B \rangle = 10^{15}\text{G}$ , we show in Fig. 5 the spectrum of the magneto-elastic waves determined by an FFT performed inside the crust near the magnetic axis and equator. As for model A1, we show the spectrum in two periods of the evolution (before and after 2.5 s) in order to identify the long lived oscillations. The properties of the spectrum appear similar to the unstratified model A1, as there is the same sequence of modes albeit at different frequencies. However, for the same magnetic field strength of model A1, an effective 2D-FFT of the various modes shows that the magneto-elastic waves in model S also permeate the crust and can be potentially relevant for the identification of the observed QPOs. This feature is shown in Fig. 6 for some of the magneto-elastic oscillations. The penetration of global oscillations into the crust may be due to the smaller difference between the Alfvén and shear velocities at the crust/core interface (Gabler et al. 2013). The two lower panels of Fig 6 show the 2D-FFT of two magneto-elastic waves that we term  $a^{(+)}$  and  $a^{(-)}$ , re-

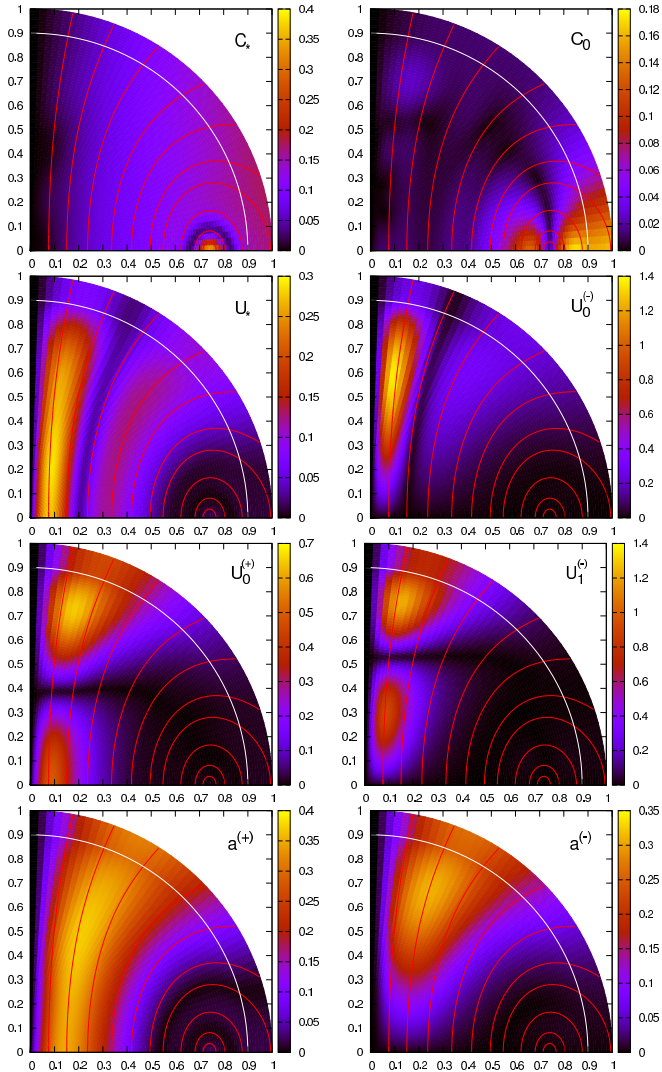


**Figure 6.** This figure shows the effective 2D-FFT of eight low frequency magneto-elastic waves for model S, whose spectrum is shown in Fig. 5. The four left-hand panels (from the top) display the  $C_*$ ,  $U_*$ ,  $U_0^{(+)}$  and  $a^{(+)}$  modes, while the four right-hand panels (from the top) show  $C_0$ ,  $U_0^{(-)}$ ,  $U_1^{(-)}$  and  $a^{(-)}$ . The red curves denote the magnetic field lines and the white curve the crust/core transition.

spectively. Their frequencies are near the  $U_*$  and  $U_0^{(+)}$  QPOs and might be identified in principle with the lower QPOs  $L_*$  and  $L_0^{(+)}$ . Their oscillation pattern, however, is not related to the last open field lines and reaches the star’s surface. Furthermore, their frequencies scale with the magnetic field and not with the shear modulus. For these reasons, we prefer to name them differently, as they could be either discrete Alfvén modes (Colaiuda & Kokkotas 2011) or  $L_n$  oscillations with magnetic modified pattern.

We have also explored the effect of composition gradients using model A2. Unlike model S, this also has a gas of superfluid neutrons in the inner crust. For the same initial conditions of model S, we consider a star with  $B_p = 5.4 \cdot 10^{14}$  G which corresponds to an average magnetic field  $\langle B \rangle = 10^{15}$  G. Rather similarly to models S and A1, we found several peaks in the early part of the simulation, including

some of crustal origin. However, these crustal oscillations were quickly absorbed leaving edges of the continuum as usual. More details on these oscillations are given in Sec. 6.3. A frequency comparison of models A1, A2 and S may be found in Table 3.

### 6.3 Effects of entrainment

As described in Section 5.1, entrainment represents a coupling between the neutral and charged components of a neutron star, which would otherwise move independently. In this subsection, we explore the oscillation spectrum of our model A3, which combines the effects of composition stratification and entrainment, as shown in Fig. 1. It is worth noticing that  $\varepsilon_*$  is larger and smaller than unity, respectively, in the core and the inner crust. Therefore, we expect an opposite effect on the magnetic- and elastic-dominated modes. The former which are located mainly in the core should be shifted at larger frequencies with respect to a zero entrainment model, while the shear modes move towards the lower frequency band. Since  $\varepsilon_*$  is not constant we expect that each mode should perceive a different value of entrainment which depends on the region where the mode is predominantly located.

The results of a long simulation ( $t \sim 6$  s) for a model with  $B_p = 5.4 \cdot 10^{14}$  G are shown in the left-hand panel of Fig. 7. As expected, the  $U_n$  and  $C_n$  QPOs appear at higher frequencies than model A2 (see Table 3), while between the  $U_n^{(-)}$  frequencies we notice some smaller amplitude peaks which appear near the crustal modes frequencies of a non-magnetised star. From the effective 2D-FFT, we find that these peaks have an intermediate character between a purely crustal and core mode, and therefore we denote them  ${}^l t_n^*$ . It is important to stress however that they are global oscillations and not crustal modes. In fact, these  ${}^l t_n^*$  oscillations have an eigenfunction pattern with a complex structure. Perpendicular to the magnetic field lines, the number of nodes is identical to an unmagnetised torsional crustal mode  ${}^l t_n$ , while along the field lines, it is equal to the next higher frequency  $U_n$  QPO. The origin of their oscillation pattern may be due to the smaller difference between the Alfvén and shear velocities at the crust/core boundary in model A3, which facilitates an energy transfer of the initial crust excitation to several open magnetic field lines. In Fig. 8, we show the effective 2D-FFT for a series of eight selected magneto-elastic waves from  $U_0^{(-)}$  to  ${}^5 t_1^*$ . As Fig. 7 shows the various  ${}^l t_n^*$  oscillations are gradually damped during the evolution. An exception is  ${}^2 t_0^*$  which is the strongest peak also during the later time interval. This might be due to its position between the  $U_0^{(-)}$  and  $U_1^{(-)}$  — presumably a continuum gap.

This suggests that at higher field strengths, more  ${}^l t_0^*$  modes may become long-lived. To check this, we also study a model with field  $B_p = 2.37 \cdot 10^{-3} \sqrt{G \rho_0} R$  ( $B_p = 1.35 \cdot 10^{15}$  G for the fiducial model). As shown in the right-hand panel of Fig. 7, the  $U_n$  QPOs now have higher frequency and the  ${}^4 t_0^*$  and  ${}^6 t_0^*$  oscillations are between the  $U_0^{(-)}$  and  $U_1^{(-)}$  frequencies. These  ${}^l t_0^*$  do indeed seem to last longer than the previous model with weaker magnetic field, and suggest the possibility that some of the low frequency QPOs actually observed may be these magneto-elastic  ${}^l t_0^*$  oscillations. Note

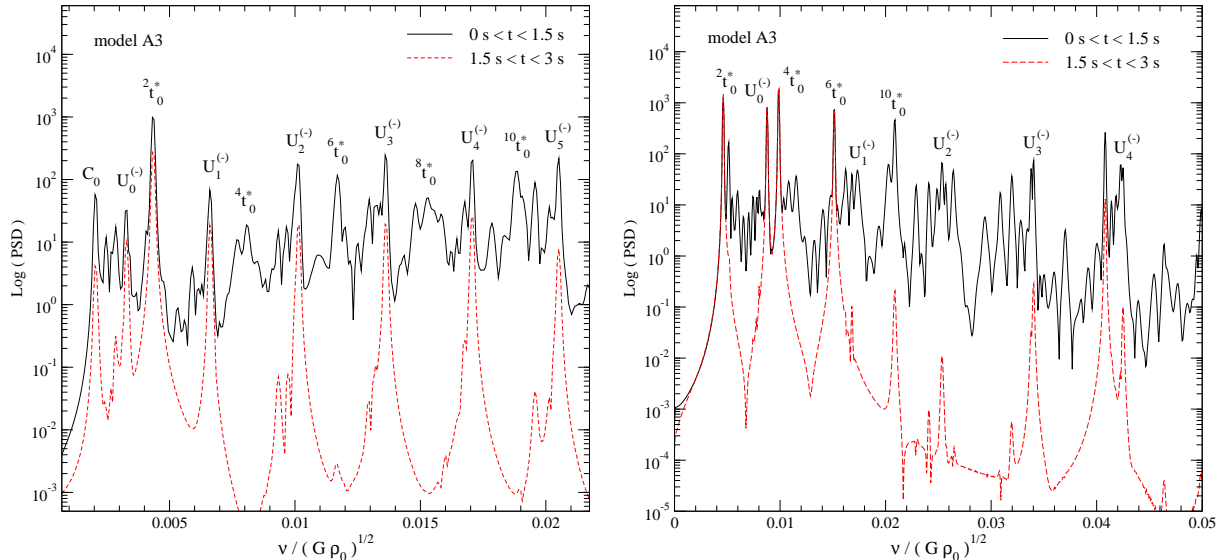


**Figure 7.** Axial axisymmetric spectrum of the magneto-elastic modes for model A3, with composition gradients and a strong entrainment in the inner crust (Chamel model). This figure shows the FFT of the antisymmetric oscillations (with respect to the equator) extracted inside the star at  $r = 0.933$  and  $\theta = 1.505$  for two distinct periods. The dashed black line denotes the FFT for  $t \lesssim 1.5$ s, the dot-dashed red line denotes the spectrum for  $1.5 \lesssim t \lesssim 3$ s. The left-hand panel displays the spectrum for a magnetic field  $B_p = 5.4 \cdot 10^{14}$ G, while the right-hand panel shows the  $B_p = 1.35 \cdot 10^{15}$ G case. The physical values for the time and  $B$ -field are referred to a star with  $M = 1.4M_\odot$  and  $R = 10$ km.

however that the  ${}^4t_0^*$  and  ${}^6t_0^*$  oscillations now have both a single node along the magnetic field line instead of, respectively, two and three nodes as for the  $B_p = 5.4 \cdot 10^{14}$ G case shown in Fig. 8.

At higher frequencies where the overtones of non-magnetised shear modes reside we find several  ${}^l t_n^*$  oscillations similar to what is observed for the fundamental modes. This means that the crustal mode overtones are also able to excite global oscillations, which in the core have high numbers of nodal lines. An example is shown in Fig. 8 for  ${}^2 t_1^*$  and  ${}^5 t_1^*$  modes, which have, respectively, dimensionless oscillation frequencies  $\nu = 0.0675\sqrt{G\rho_0}$  and  $0.0678\sqrt{G\rho_0}$ . In the crust, we can recognise a radial nodal line of an  $n = 1$  crustal mode which excites a very high overtone of a core magnetic mode. In order to appreciate this effect, a simulation with higher radial resolution is needed. We used in this case a  $48 \times 120$  grid resolution. This behaviour, already reported in Gabler et al. (2013), confirms the different behaviour of QPOs in superfluid neutron stars. However, it would be important to determine the duration of these oscillations in order to explain the higher frequency QPOs observed in the tail of SGR 1806-20 with 625 and 1837 Hz, which, respectively, lasted about 200 and 15 s. With the current resolution, we are not able to provide a secure answer to this question.

#### 6.4 QPO interpretation

The observed QPOs can be roughly divided into a set of low- and high-frequency QPOs. In fact, the majority of the frequencies reside in the band  $\nu < 155$  Hz, with only two outside this range, at 625 and 1837Hz — both detected from SGR1806-20. We wish to examine our results in the context of these observations, to see which model stellar parameters

are required to provide oscillations in the appropriate range. Our goal here is not to determine a model that strictly fits all the observed frequencies, as our stars are still rudimentary in many respects. In particular, it would be more appropriate to use realistic EoSs instead of polytropes to explore the neutron star parameter space. This problem will also require a proper description of gravity in general relativity and will be addressed in future work. With our current models, we can however understand the effects of composition stratification and entrainment on the spectrum and their influence on the magnetic field strength required to explain the observations.

For our models we consider a standard mass  $M = 1.4M_\odot$  and vary the radius in order to tune the QPOs' frequency range. This choice will determine at the same time the transformation relation from the dimensionless to the physical units for the frequency and magnetic field strength.

Let us start with model S and consider a radius  $R = 10$  km and two possible magnetic field strengths, namely  $B_p = 3.3 \cdot 10^{14}$ G and  $B_p = 8.3 \cdot 10^{14}$ G, which, respectively, correspond to an average magnetic field  $\langle B \rangle = 10^{15}$ G and  $\langle B \rangle = 2.5 \cdot 10^{15}$ G. Note that in model S, the field is more buried than for model A, with an interior field about three times that at the polar cap. Already for these intermediate magnetic fields, the magneto-elastic waves of model S penetrate the crust in both the open and closed field line regions. This is a crucial property in the current paradigm for the interpretation of QPOs as a result of the modulation of a trapped fireball by crustal vibrations (Thompson & Duncan 1995).

As Table 4 shows, even at a relatively low field of  $B_p = 3.3 \cdot 10^{14}$ G many  $C_n$  and  $U_n$  QPOs provide an approximate match to the observations: for instance  $U_0^{(+)} \simeq 18$ Hz,  $U_1^{(-)} \simeq 26$ Hz,  $C_1 \simeq 30$ Hz, while the higher overtone of

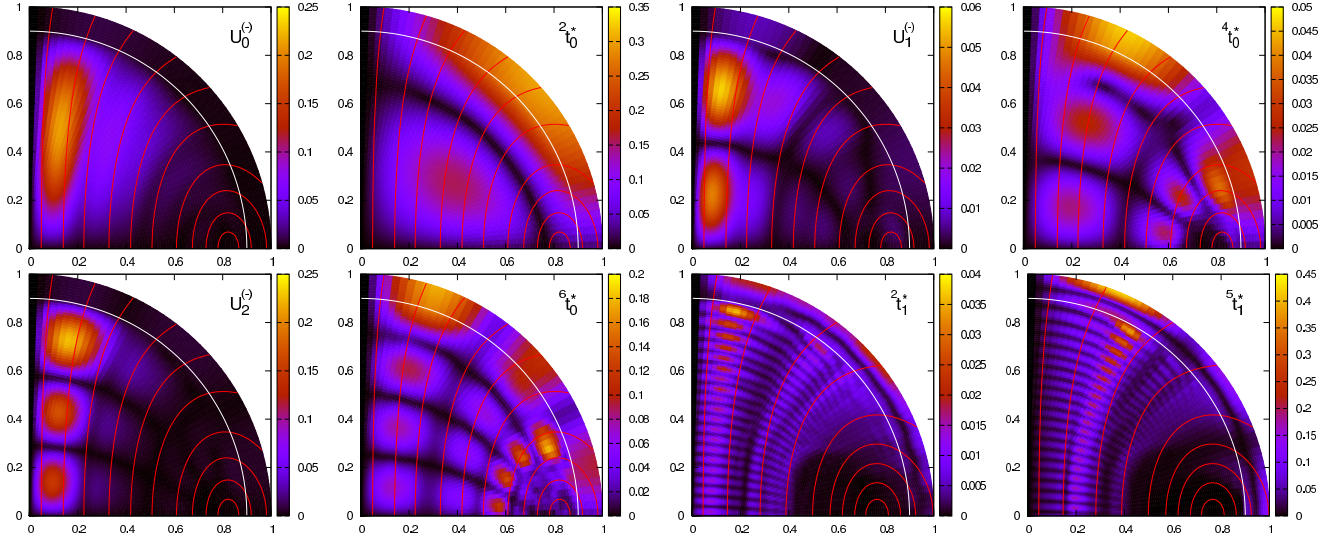


**Figure 8.** This figure shows the effective 2D-FFT of eight magneto-elastic oscillations for model A3 with magnetic field  $B_p = 5.4 \cdot 10^{14}$  G. The four upper panels show (from the left):  $U_0^{(-)}$ ,  $2t_0^*$ ,  $U_1^{(-)}$  and  $4t_0^*$ , and the four lower panels show (from the left):  $U_2^{(-)}$ ,  $6t_0^*$ ,  $2t_1^*$  and  $5t_1^*$ .

**Table 4.** Potentially observable magneto-elastic oscillations from model S. The frequencies are given in Hz for a model S with  $M = 1.4M_\odot$  and  $R = 10$  km. The averaged magnetic field and its value at the pole are given in gauss in the second and third columns, respectively. These frequencies may be rescaled for a star with a different radius by using  $\nu \sim R^{-3/2}$ .

Model	$\langle B \rangle$	$B_p$	$C_0$	$C_1$	$C_2$	$a^{(+)}$	$a^{(-)}$	$U_*$	$U_0^{(-)}$	$U_0^{(+)}$	$U_1^{(-)}$	$U_1^{(+)}$
S	$1.0 \cdot 10^{15}$	$3.3 \cdot 10^{14}$	15.4	29.9	44.7	5.7	11.4	7.0	12.8	18.7	25.6	32.6
S	$2.5 \cdot 10^{15}$	$8.3 \cdot 10^{14}$	38.4	74.3	111.4	11.3	24.6	14.6	29.9	42.7	59.6	76.9

$U_n$  frequencies can describe the other QPOs at  $< 155$  Hz. A similar identification can be found with model S and  $B_p = 8.3 \cdot 10^{14}$  G. This numerology is, of course, a little arbitrary at this stage — one might instead choose to associate our lowest-frequency mode,  $a^{(+)}$ , with the lowest-frequency reported QPO: the 16.9 Hz frequency found from a recent re-analysis of the SGR1806-20 data (Hambaryan et al. 2011).

For model A3 the QPO frequency range is better described by a star with  $R = 14$  km. In contrast with model S, the  $C_n$  oscillations are confined in the core for intermediate magnetic fields, but due to the strong entrainment at the bottom of the inner crust many  ${}^l t_0^*$  oscillations appears at low frequencies and live longer. In Table 5 we show the QPO frequencies for two magnetic fields,  $B_p = 2.8 \cdot 10^{14}$  G and  $B_p = 6.9 \cdot 10^{14}$  G. For the latter case, the  $U_n$  oscillations penetrate the crust and hence are suitable for association with observed QPOs. In this case however we see from Table 5 that the  $U_n$  oscillations cannot explain the very lowest frequency QPO (16.9 Hz). An intriguing possibility to explore for model A3 is the case of  $B_p > 10^{15}$  G and a smaller shear modulus. The spectrum at low frequencies might be populated more by  ${}^l t_0^*$  oscillations, while the  $U_n$  QPOs would be shifted at higher frequencies. Many of the low QPOs could be interpreted with a series of  ${}^l t_0^*$  oscillations similar to those already proposed initially for unmagnetised models. In particular, it would be interesting to investigate this possibility by adding the effect of magnetic fields to the analysis of Steiner & Watts (2009).

From these preliminary results it is evident that in superfluid magnetar models the poloidal magnetic field required to describe the QPO spectrum is weaker than in normal fluid stars. This is an expected outcome which comes from the different definition of the Alfvén speed in these two systems. Another interesting feature of superfluid models could be the identification of the two high-frequency QPOs. In the standard single-fluid model, these two high frequency QPOs have been hard to explain, due to the resonant absorption of the highly dense magnetic core oscillations (van Hoven & Levin 2011, 2012). In the superfluid case, the higher frequency QPOs could represent overtones of the  ${}^l t_n^*$  oscillations, as recently proposed by Gabler et al. (2013): the smaller difference between the Alfvén and shear speed at the crust/core interface should facilitate a resonance between the crust and the core oscillations. For instance for model A3 with  $\langle B \rangle = 10^{15}$  G we find that the  ${}^l t_1^*$  may vary within (490, 811) Hz,  ${}^l t_2^*$  within (877, 1453) Hz and  ${}^l t_3^*$  in (1243, 2059) Hz. The lower and upper limits of the oscillation frequencies correspond to stellar models with, respectively,  $R = 14$  and 10 km. In order to assess the duration of these oscillations and therefore their relevance for the QPO identification one requires a high-resolution numerical grid, as at these frequencies the core oscillations have a large number of nodal lines. The solution of this question is beyond our current numerical capabilities, but we hope to return to it in the future.

Another possibility is that the high-frequency QPOs are

**Table 5.** Potentially observable magneto-elastic oscillations from models A2 and A3. The frequencies are given in Hz for models with  $M = 1.4M_\odot$  and  $R = 14$  km. As in the last table, the averaged magnetic field and its value at the pole are given in gauss in the second and third column, respectively. These frequencies may be rescaled for a star with a different radius by using  $\nu \sim R^{-3/2}$ . The upper index \* denotes oscillations which are damped in  $t < 1s$ , while the † indicates magneto-elastic waves which do not penetrate the crust.

Model	$\langle B \rangle$	$B_p$	${}^2t_0^*$	${}^3t_0^*$	${}^4t_0^*$	$C_0$	$U_*$	$U_0^{(-)}$	$U_0^{(+)}$	$U_1^{(-)}$	$U_1^{(+)}$
A2	$5.3 \cdot 10^{14}$	$2.8 \cdot 10^{14}$	49.0*	—	104.6*	13.5†	9.1†	18.8†	28.5†	38.7†	47.4†
A3	$5.3 \cdot 10^{14}$	$2.8 \cdot 10^{14}$	31.9	47.8	—	15.1	10.3†	24.4†	36.7†	49.2†	61.9†
A3	$1.3 \cdot 10^{15}$	$6.9 \cdot 10^{14}$	33.6	40.5	72.5	—	26.7	64.0	94.2	123.9	148.6

non-axisymmetric magnetic modes of the superfluid core. For surface fields of the order of  $10^{15}$  G, we found that the 150 and 625 Hz QPOs of SGR1806-20 and the 155 Hz QPO of SGR1900+14 could plausibly be ‘fundamental’  $m = 2$  Alfvén oscillations (Passamonti & Lander 2013). Even in this scenario, however, the 1837 Hz frequency would have to be some kind of higher order mode — either an overtone or a mode with  $m > 2$ .

## 7 DISCUSSION

The original discovery of magnetar QPOs, in the right frequency range to be shear modes of the crust, brought hopes of probing the neutron star interior and constraining the EoS of dense matter. These hopes have been somewhat diluted, as it has become clear that more physics is at play in magnetar QPOs than simply the star’s elastic crust. On the other hand, these complications mean that there is potentially additional information to be gleaned from these observations: the magnetic field structure within a neutron star and the nature of any superfluid/superconducting components.

The entirety of observations to date consist of two sets of data: the decaying X-ray tails that followed the giant flares of two soft gamma repeaters. These tails are clearly modulated at the rotation rate of each star; it has been suggested that what we see is a fireball above the star but anchored to its surface (Thompson & Duncan 1995). If the observed QPOs do indeed correspond to oscillations of the star, these must also be propagated from the surface through this fireball. The QPOs themselves cover a frequency band from tens of Hz up to kHz, many of them only appearing in certain parts of the X-ray tail.

In this work, we attack the problem of modelling magnetar QPOs by looking at the behaviour of linearised perturbations of a magnetised star, accounting for the effect of superfluid neutrons and an elastic crust. This clearly only addresses part of the phenomenology described above — indeed, the best-studied part of it — attempting to link the frequencies of observed QPOs to different classes of stellar oscillation. Nonetheless, we can still learn something from this endeavour.

In a magnetar with a single-fluid crust and two-fluid core with composition stratification, we find that many magnetic oscillations are able to penetrate the crust and could explain the lowest frequency observed QPOs, 17-18Hz, as well as others in the range up to  $\sim 150$  Hz. In a magnetar model with superfluid neutrons both in the inner crust and the core, the strong crustal entrainment reduces the frequencies of the shear modes. As a result, a new series of

magneto-elastic waves with hybrid character appears. For a typical magnetar field strength ( $B_p \sim 10^{15}$  G) they have frequency close to that of shear modes of a unmagnetised model, but their oscillation pattern is not localised into the crust. We call these global oscillations  ${}^l t_n^*$  in order to recall their analogy with crustal axial modes (torsional modes).

In superfluid models with strong entrainment in the crust and  $B_p \sim 10^{15}$  G, the frequency range  $25 \lesssim \nu \lesssim 150$  Hz contains a number of  ${}^l t_n^*$  modes which are not damped by coupling with the core, in contrast with the shear waves of the single-fluid case. Moreover, the overtones of  ${}^l t_n^*$  oscillations appear at higher frequencies and could explain QPOs in the range  $150 \lesssim \nu \lesssim 2000$  Hz. This result is in agreement with the recent work of Gabler et al. (2013) Numerical limitations however prevent us from reliably determining their duration. In our current models with superfluid neutrons in the crust, QPOs below  $\sim 25$  Hz become harder to explain if a ‘standard’ shear modulus value and typical magnetar field strengths are used.

Recent results from Gabler et al. (2013) find discrete Alfvén modes in a superfluid star, replacing the continuous spectrum of single-fluid models. In an attempt to confirm this result, we have studied also the behaviour of the QPO phase in our stellar models to determine the discrete/continuum nature of the spectrum. Unfortunately, our results do not provide conclusive evidence that the spectrum is fundamentally different in the superfluid case. This is certainly a problem which deserves more accurate investigation in future work.

Our current Newtonian polytropic models are able to describe the properties of many magnetar QPOs, even with a relatively low dipolar magnetic field, depending on the particular model. It would be possible to ‘tune’ our results to the observed data and find a fit for each observed frequency. Nonetheless, with so many degrees of freedom at play, we do not think any reliable conclusions could be drawn from this approach. Instead, a more detailed analysis of the parameter space will be carried out in a future work where also relativistic effects and tabulated EoSs will be considered.

Important physics typically missing from studies of the dynamical-timescale problem of linearised oscillations include the effect of proton superconductivity and the fact that magnetars may not be old enough for neutrons to have condensed into a superfluid throughout the core, but only in regions. Like the effect of entrainment, this would tend to reduce the superfluid enhancement of Alfvén frequencies. For example, one might naively assume that magnetic oscillations of SGR1900+14 should be of lower frequency than the corresponding oscillations of SGR1806-20, since the former

magnetar has a lower inferred dipole field. It is also an order of magnitude older (Tendulkar et al. 2012), however, so its core should contain a larger region with superfluid neutrons — and its oscillations would then be *higher* in frequency.

Perhaps a more pressing problem is explaining why some QPOs appear and disappear in the middle of the tail but others survive for hundreds of seconds. This might involve studying possible mode couplings to see if some oscillations maintain their energy at the expense of others. More detailed modelling is clearly also required to explain the locally heated, post-flare magnetosphere of the magnetar and how stellar oscillations propagate through this to become visible to us.

### ACKNOWLEDGEMENTS

AP acknowledges support from the European Union Seventh Framework Programme (FP7/2007-2013) under grant agreement no. 267251 “Astronomy Fellowships in Italy (AstroFit)”. SL acknowledges support from the German Science Foundation (DFG) via SFB/TR7. We would like to thank A. Colaiuda, M. Gabler, K. Kokkotas, L. Stella and N. Stergioulas for fruitful discussions and comments.

### APPENDIX A: WAVE EQUATION COEFFICIENTS

We write here the coefficients of the wave equation (14):

$$A_1 = \mu + \frac{B_r^2}{4\pi}, \quad (\text{A1})$$

$$A_2 = \frac{\mu}{r^2} + \frac{B_\theta^2}{4\pi r^2}, \quad (\text{A2})$$

$$A_3 = \frac{B^r B^\theta}{2\pi r}, \quad (\text{A3})$$

$$A_4 = \frac{2\mu}{r} + \frac{d\mu}{dr} + \frac{1}{4\pi r} \left[ B^\theta \partial_\theta B^r - B^r (2B^r + \partial_\theta B^\theta + \cot \theta B^\theta) \right], \quad (\text{A4})$$

$$A_5 = \frac{\mu \cot \theta}{r^2} + \frac{1}{4\pi r^2} \left[ B^\theta (\partial_\theta B^\theta - B^r) + r B^r \partial_r B^\theta \right], \quad (\text{A5})$$

$$A_6 = -\frac{\mu}{r^2 \sin^2 \theta} - \frac{1}{r} \frac{d\mu}{dr} + \frac{1}{4\pi r^2} \left[ B^r (2B^r + \partial_\theta B^\theta - r \cot \theta \partial_r B^\theta) + B^\theta (B^\theta - \partial_\theta B^r - \cot \theta \partial_\theta B^\theta) \right]. \quad (\text{A6})$$

In the limit of zero shear modulus  $\mu = 0$ , the quantities  $A_k$  become the coefficients of the wave equation for the core’s protons.

### REFERENCES

Andersson N., Glampedakis K., Samuelsson L., 2009, MNRAS, 396, 894  
 Andersson N., Haskell B., Samuelsson L., 2011, MNRAS, 416, 118  
 Cerdá-Durán P., Stergioulas N., Font J. A., 2009, MNRAS, 397, 1607  
 Chamel N., 2008, MNRAS, 388, 737

Chamel N., 2012, Phys. Rev. C, 85, 035801  
 Colaiuda A., Beyer H., Kokkotas K. D., 2009, MNRAS, 396, 1441  
 Colaiuda A., Kokkotas K. D., 2011, MNRAS, 414, 3014  
 Colaiuda A., Kokkotas K. D., 2012, MNRAS, 423, 811  
 Douchin F., Haensel P., 2001, A&A, 380, 151  
 Duncan R. C., 1998, ApJ, 498, L45  
 Gabler M., Cerdá Durán P., Font J. A., Müller E., Stergioulas N., 2011, MNRAS, 410, L37  
 Gabler M., Cerdá-Durán P., Stergioulas N., Font J. A., Müller E., 2012, MNRAS, 421, 2054  
 Gabler M., Cerdá-Durán P., Stergioulas N., Font J. A., Müller E., 2013, Phys. Rev. Lett., 111, 211102  
 Glampedakis K., Samuelsson L., Andersson N., 2006, MNRAS, 371, L74  
 Glampedakis K., Andersson N., Samuelsson L., 2011, MNRAS, 410, 805  
 Hambaryan V., Neuhäuser R., Kokkotas K. D., 2011, A&A, 528, A45  
 Ho W. C. G., Glampedakis K., Andersson N., 2012, MNRAS, 422, 2632  
 Israel G. L., Belloni T., Stella L., Rephaeli Y., Gruber D. E., Casella P., Dall’Osso S., Rea N., Persic M., Rothschild R. E., 2005, ApJ, 628, L53  
 Lander S. K., Andersson N., Glampedakis K., 2012, MNRAS, 419, 732  
 Levin Y., 2006, MNRAS, 368, L35  
 Levin Y., 2007, MNRAS, 377, 159  
 Passamonti A., Andersson N., 2012, MNRAS, 419, 638  
 Passamonti A., Haskell B., Andersson N., 2009, MNRAS, 396, 951  
 Passamonti A., Lander S. K., 2013, MNRAS, 429, 767  
 Samuelsson L., Andersson N., 2007, MNRAS, 374, 256  
 Samuelsson L., Andersson N., 2009, Class. Quantum Grav., 26, 155016  
 Sauls J., 1989, in Ögelman H., van den Heuvel E. P. J., eds, Timing Neutron Stars. Springer-Verlag, Berlin, p. 457  
 Sotani H., Kokkotas K. D., Stergioulas N., 2008, MNRAS, 385, L5  
 Sotani H., Nakazato K., Iida K., Oyamatsu K., 2013, MNRAS, 428, L21  
 Steiner A. W., Watts A. L., 2009, Phys. Rev. Lett., 103, 181101  
 Stergioulas N., Apostolatos T. A., Font J. A., 2004, MNRAS, 352, 1089  
 Strohmayer T. E., Watts A. L., 2005, ApJ, 632, L111  
 Tendulkar S. P., Cameron P. B., Kulkarni S. R., 2012, ApJ, 761, 76  
 Thompson C., Duncan R. C., 1995, MNRAS, 275, 255  
 Thompson C., Duncan R. C., 1996, ApJ, 473, 322  
 van Hoven M., Levin Y., 2008, MNRAS, 391, 283  
 van Hoven M., Levin Y., 2011, MNRAS, 410, 1036  
 van Hoven M., Levin Y., 2012, MNRAS, 420, 3035